Cell. Mol. Life Sci. 64 (2007) 1970 – 1978
1420-682X/07/151970-9
DOI 10.1007/s00018-007-6514-3

Cellular and Molecular Life Sciences

Review

Selectivity determinants of the aldose and aldehyde reductase inhibitor-binding sites

O. El-Kabbani[a, *] and A. Podjarny[b]

[a]Department of Medicinal Chemistry, Victorian College of Pharmacy, Monash University (Parkville Campus), 381 Royal Parade, Parkville, Victoria 3052 (Australia), Fax: +61 3 9903 9582,
e-mail: ossama.el-kabbani@vcp.monash.edu.au
[b]Department of Structural Biology and Genomics, IGBMC, ULP, INSERM, UMR 7104 du CNRS, 1 rue Laurent Fries, 67404 Illkirch (France)

Received 4 December 2006; received after revision 12 February 2007; accepted 20 April 2007
Online First 11 May 2007

Abstract. Aldose reductase and aldehyde reductase belong to the aldo-keto reductase superfamily of enzymes whose members are responsible for a wide variety of biological functions. Aldose reductase has been identified as the first enzyme involved in the polyol pathway of glucose metabolism which converts glucose into sorbitol. Glucose over-utilization through the polyol pathway has been linked to tissue-based pathologies associated with diabetes complications, which make the development of a potent aldose reductase inhibitor an obvious and attractive strategy to prevent or delay the onset and progression of the complications. Structural studies of aldose reductase and the homologous aldehyde reductase in complex with inhibitor were carried out to explain the difference in the potency of enzyme inhibition. The aim of this review is to provide a comprehensive summary of previous studies to aid the development of aldose reductase inhibitors that may have less toxicity problems than the currently available ones.

Keywords. Aldose reductase, aldehyde reductase, polyol pathway, glucose metabolism, enzyme inhibition, drug design, diabetes.

Aldose reductase (ALR2; EC 1.1.1.21) and aldehyde reductase (ALR1; EC 1.1.1.2) belong to the aldo-keto reductase (AKR) superfamily of enzymes whose members are responsible for a wide variety of biological functions. These include the regulation of the pro-inflammatory response via the reduction of aldehyde phospholipids [1], the synthesis of metabolically vital compounds such as prostaglandins [2, 3] and the modulation and modification of steroids *in vivo* [4–7], which include progesterone signalling in breast mammary cells [8]. Members of the AKR superfamily are composed of approximately 315–330 residues, which generally form monomeric proteins with a molecular weight of 36 kDa [9, 10]. While ALR1 prefers the reduction of aromatic rather than aliphatic aldehydes [11], both ALR1 and ALR2 catalyse the NADPH-dependent reduction of aldehydes, xenobiotic aldehydes, ketones, trioses and triose phosphates [9, 10, 12–15]. The two enzymes have been isolated and purified from a number of tissues including the brain, kidney, liver, lens and skeletal muscle [16–18]. ALR2 is the first enzyme in the polyol pathway and converts glucose to sorbitol, which is subsequently transformed

* Corresponding author.

to fructose by sorbitol dehydrogenase. During a hyperglycaemic event, the elevated glucose level enhances ALR2 activity, increasing the glucose flux through the polyol pathway which impacts other NADPH-dependent enzymes shown to play a key role in long-term diabetic onset complications such as neuropathy and nephropathy [19]. Moreover, the consequent accumulation of sorbitol in the eye is believed to be responsible for the development of glaucoma, retinopathies and cataracts in diabetic patients [20]. Inhibition of ALR2 thus offers patients suffering from diabetes mellitus a viable therapeutic measure against the debilitating pathologies associated with chronic hyperglycaemia [21–23]. While many aldose reductase inhibitors (ARIs) have been reported in the literature, adverse side effects and lack of efficacy have curtailed the prospect of many drug candidates for clinical use. Epalrestat is the only ARI that is currently marketed for treatment of diabetic neuropathy in Japan, with several other potential candidates in current clinical trials [23–25].

ALR1 and ALR2 share a high degree of sequence (~65%) and structural homology [26], with the majority of the differences present at the C-terminal end of an α/β-TIM barrel structure (Fig. 1) [27], which is the region mainly responsible for substrate and inhibitor specificity among members of the AKR superfamily [28]. Earlier studies indicated that most known ALR2 inhibitors inhibit ALR1 and illustrated that the active sites of both enzymes contain common characteristics in the manner in which they bind substrate and inhibitor [26, 29]. An ARI specificity is often determined by measuring its activity against ALR1, an enzyme that metabolizes 3-deoxyglucosone and methylglyoxal which are intermediates for the formation of the advanced glycation end products (AGEs) [30, 31]. Thus, ALR1 inhibition may account for some of the undesirable side effects associated with the present ARIs. It is therefore necessary to identify any structural differences between these enzymes that may be exploited in the design of inhibitors that are highly selective for ALR2 over ALR1.

Traditionally, ARIs emerged from two major classes, depending on whether they contain an acetic acid moiety [32] or a cyclic imide group. The latter in turn comprises hydantoin/imidazoline-2,4-dione derivatives [33], such as Fidarestat and Sorbinil, or succinimide derivatives [34], like Minalrestat and AS-3201. These polar groups are usually attached to a hydrophobic ring system [22]. X-ray structures of several ALR2-inhibitor complexes showed that the polar hydantoin and carboxylate groups bind in a conserved anion-binding site adjacent to the nicotinamide ring of the coenzyme. They form hydrogen bonds with ALR2

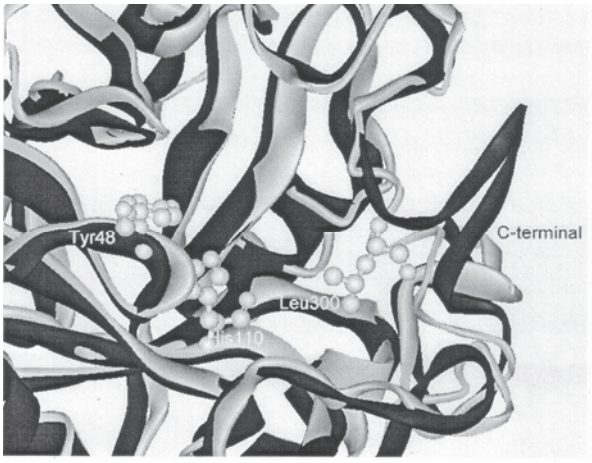

Figure 1. Superposition of aldose reductase (white ribbon) and aldehyde reductase (black ribbon). Note that the two structures are very close except at the C-terminal end. The active site is marked by catalytic residues Tyr48 and His110. Leu300 (Pro in aldehyde reductase) marks the beginning of the C-terminal end.

residues Tyr48, His110 and Trp111 [33, 35]. Inhibitors containing either the cyclic imide or carboxylic acid anchor exhibit similar *in vitro* but lower *in vivo* activity with respect to the carboxylic acid derivatives. This observation has been attributed to the relatively lower pK_a values and, accordingly, their ionization at physiological pH [36–38]. Most ALR2 inhibitors are also effective against ALR1 because they bind to the enzyme in a very similar manner, with the polar inhibitor moiety wedged between the nicotinamide ring and the conserved residues Tyr48, His110 and Trp79 [35, 39, 40]. The hydrophobic ring systems of the inhibitors are bound tightly in a pocket that is adjacent to the anion-binding site. Inhibition and biochemical studies have suggested that inhibitors with different potencies for ALR1 and ALR2 are likely to interact with residues in the C-terminal loop [28, 39], since this portion is not conserved across members of the aldo-keto reductase superfamily [41]. Moreover, crystallographic and modelling studies of ALR1 and ALR2 in complex with inhibitors have shown that inhibitors specific to ALR2 interact with C-terminal residues by binding to the same subsite, which has been described as the 'specificity' pocket [33, 35, 42].

In this review we compare the three-dimensional (3D) structures of ALR1 and ALR2 in complex with the cyclic imide inhibitor Fidarestat {(2*S*,4*S*)-6-fluoro-2′,5′-dioxospiro-[chroman-4,4′-imidazoline]-2-carboxamide} complemented with data obtained from molecular modelling calculations and inhibitory activity measurements to illustrate the selectivity-determining features that may be used in a rational approach to the drug design process [43–46].

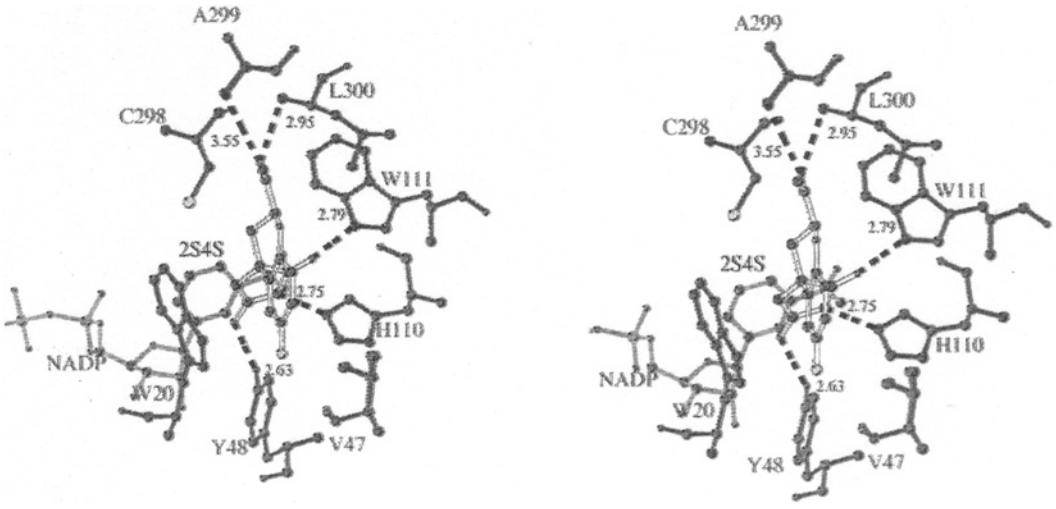

Figure 2. Stereoview of Fidarestat bound into the active site of human ALR2. Residues within 4 Å of the inhibitor are shown. Hydrogen bonds (dashed lines) are drawn between the inhibitor and His110 Nε2, Tyr48 OH, Trp111 Nε1 and Leu300 N, with distances given in Å.

Structure of the ALR2/Fidarestat complex

A stereo diagram of Fidarestat bound to the active site of ALR2 is presented in Figure 2. The overall structure of human ALR2 folds into an eight-stranded α/β-barrel with the active site located on the C-terminal end of the barrel [47]. The $NADP^+$-binding site is located adjacent to a hydrophobic active site pocket. As previously observed in crystal structures of ALR2 in complex with hydantoin inhibitors [33, 35], Fidarestat is bound in the active site with its hydantoin moiety entering the anion-binding site [44]. This moiety is held in place by 13 van der Waals interactions with the nicotinamide ring of $NADP^+$. Thus, the inhibitor's polar head is firmly anchored in the active site. Both carbonyl oxygen atoms are present within hydrogen-bonding distances from the Nε1 atom of Trp111 (2.80 Å) and the OH group of Tyr48 (2.63 Å). His110 forms a hydrogen bond with the 1′-position nitrogen atom in the cyclic imide substituent of Fidarestat (2.76 Å). Peaks in the experimental electron density obtained by X-ray diffraction clearly indicated two positions for the H atom in this bond. Furthermore, the C–O bond distances in the cyclic imide rings (1.2 Å +/- 0.04) clearly indicated a double bond, excluding the protonation of the oxygen atoms. These observations lead to the conclusion that the inhibitor can have different protonation states at the 1′-position nitrogen atom in the cyclic imide substituent [44].

While cyclic imide and carboxylic acid ARIs have comparable activities *in vitro*, the exchange of the acetic acid functional group with a cyclic imide substituent has been found to transform the compound from being exclusively active *in vitro* to a compound with high potency *in vivo* [48–50], likely due to accompanying changes in the pharmacokinetic properties of the compound, such as the pKa value. Carboxylic acids have low pKa values (generally below 4) which causes them to be ionized at physiological pH and more difficult to cross the biological membrane than cyclic imides which have higher pKa values (between 8 and 9) [37]. Interestingly, the experimentally measured pKa value (pKa ~8) for the catalytic residue Tyr48 has been shown to be approximately 2.5 units lower than the pKa value calculated for a Tyr residue in solution [51]. Similarly, the presence of the cyclic imide substituent of Fidarestat in close proximity with the positively charged nicotinamide ring of the coenzyme and the protonated Nε2 of His110 could lower the pKa value of the cyclic imide substituent, resulting in a partial population of inhibitors which would be negatively charged at the 1′-position nitrogen atom at the crystallisation pH of 5.0. Biochemical and crystallographic studies have suggested that ARIs preferably bind to the ALR2/$NADP^+$ complex whereas the substrates bind to the ALR2/NADPH form [35, 52]. At physiological pH, the inhibitor population that is negatively charged at the 1′-position nitrogen atom in the cyclic imide substituent would interact favourably with the protonated Nε2 atom of His110 and positively charged nicotinamide of the coenzyme. This suggests that cyclic imide inhibitors initially cross the biological membrane as neutral compounds, then lose the proton and bind to the enzyme's active site, with their negative charge contributing to the tight inhibitor binding. This observation is supported by the fact that the translation from *in vitro* to *in vivo* activity for this class of compounds was usually easily achieved [37, 53].

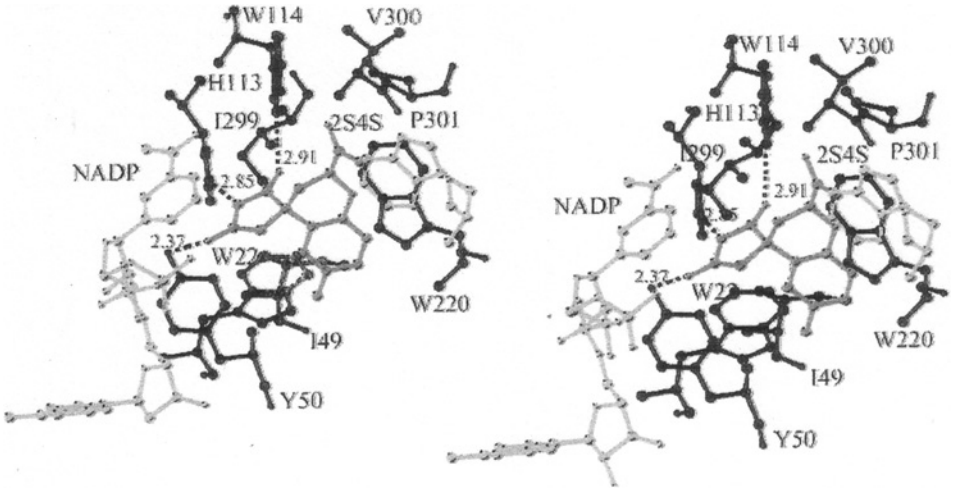

Figure 3. Stereo-diagram showing the binding site of Fidarestat to ALR1. Residues within 4 Å and hydrogen bonds as dashed lines, with distances given in Å. The two conformations for Trp 220 are included.

The orientation of the bound Fidarestat in the active site of human ALR2 holoenzyme determined at ultra-high resolution (0.9 Å) is in agreement with an earlier crystallographic investigation conducted at 2.8 Å resolution where the chroman ring of Fidarestat was located within van der Waals contacts with the side chains of Trp20, Trp111, Phe122 and Trp219 [44, 33]. The oxygen of the carbonyl group was hydrogen-bonded to the main-chain nitrogen atom of Leu300 (Leu300 adopts a double conformation in the high-resolution structure with hydrogen bond distances equal to 2.96 and 3.03 Å). This interaction was suggested to be responsible for the higher potency of Fidarestat for ALR2 over ALR1 [33]. Leu300 that lines the 'specificity' pocket in ALR2 is a Pro in ALR1 and is unable to form a hydrogen bond with the inhibitor.

Structure of the ALR1/Fidarestat complex

Fidarestat binds to the active site of ALR1 with its cyclic imide moiety anchored in the anion-binding site [43] (Fig. 3). The carbonyl oxygen atoms are present within hydrogen-bonding distances from the Nε1 atom of Trp114 (2.91 Å) and the OH group of Tyr50 (2.37 Å), while the Nε2 of His113 forms a hydrogen bond with the 1′-position nitrogen atom in the cyclic imide substituent (2.85 Å). The hydrogen-bonding interactions between the cyclic imide moiety of Fidarestat and ALR1 are conserved in the ALR2 structure which includes an additional hydrogen bond between the main-chain N atom of Leu300, a residue lining the 'specificity' pocket, and the exocyclic amide oxygen of Fidarestat [44]. A superposition of the ALR1 and ALR2 active sites with the bound Fidarestat molecules is shown in Figure 4. While the side-chain orientations for the anion-binding-site residues Tyr50, His113 and Trp114 are conserved, the experimental electron density obtained from X-ray diffraction studies indicated a disordered double conformation for the indole ring of Trp220 in ALR1 that may have resulted from a short contact interaction with the flexible exocyclic amide group, inducing the major conformation (80 % occupancy). The two conformations have van der Waals contacts with the exocyclic amide group equal to 2.99 and 3.59 Å, respectively [43]. The former short contact is likely to contribute to a less favoured inhibitor binding compared to ALR2, where a single conformation was observed that has a

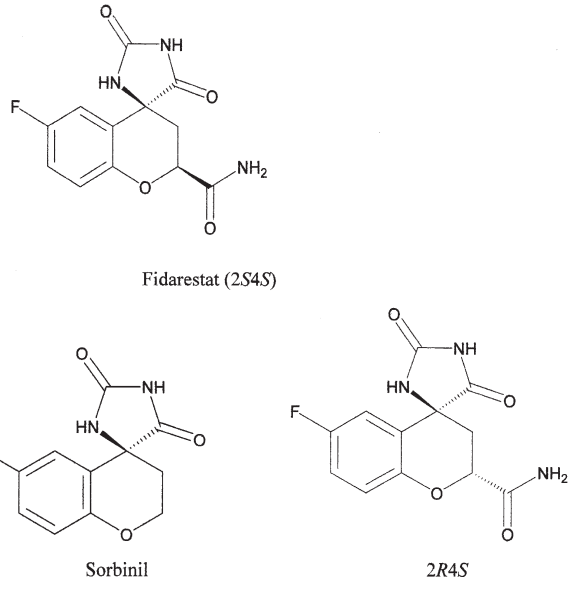

Scheme 1

Table 1. Comparisons of ALR1 and ALR2 inhibitor binding constants IC_{50} (μM) and ΔH (kcal/mol).

Inhibitor	IC_{50}. porcine ALR1	IC_{50} . human ALR1	IC_{50} . human ALR2	IC_{50}. rat . ALR2	ΔH. porcine ALR1	ΔH. human ALR2
Fidarestat	2.5	1.2[a]	0.009[a]	0.035[c]	–12	–15
Sorbinil	4.0	5.4[b]	2.0[b]	0.90[c]		
2*R*4*S*	17.8			0.57[c]		

IC_{50} values reported by [a]Mizuno et al. [55] [b]Barski et al. [56] and [c]Yamaguchi et al. [57].

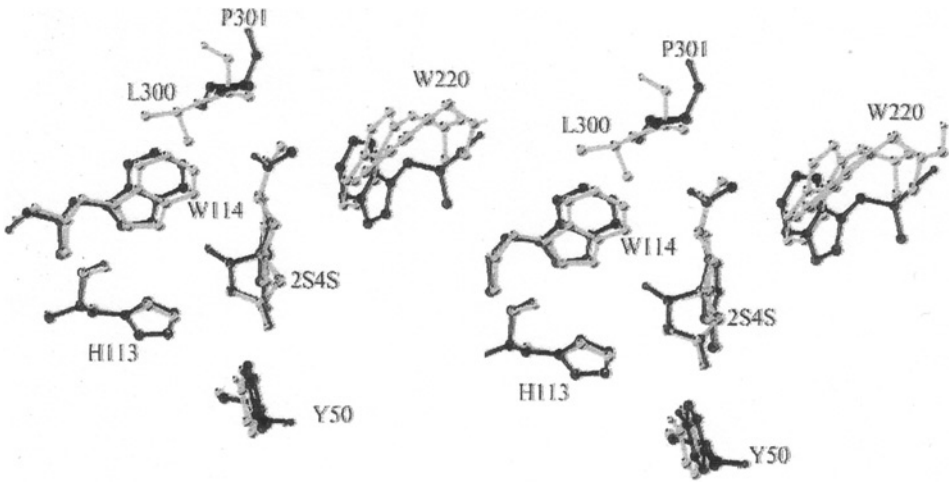

Figure 4. Superposition of the inhibitor-binding site residues Tyr50, His113, Trp114, Trp220 and Pro301 (Leu300 in ALR2) in ALR1 and ALR2.

van der Waals contact with the exocyclic amide group equal to 3.61 Å [44]. The correlation between the electrostatic component of the binding enthalpy (ΔH) and the binding constants measured in solution (IC_{50}) for Fidarestat was examined for ALR1 and ALR2. Estimates of the electrostatic interactions between the residues Tyr50, His113, Trp114 and Leu300 (Pro301 in ALR1) and the inhibitor were obtained from molecular modelling. Additionally, for comparison and to illustrate the role of the exocyclic amide group in inhibitor binding to ALR1 and ALR2, the IC_{50} values of the 2*R*4*S*-isomer and Sorbinil (Scheme 1) for the two enzymes are provided in Table 1 as a guide for inhibitor-binding affinity in solution [43].

A comparison between the structures of the ALR2 complexes with Fidarestat (2*S*4*S*) and its 2*R*4*S* isomer shows differences in the interaction between the exocyclic amide group and the C-terminal loop residues [45]. While the hydrogen bond between the exocyclic amide group of the compounds and the main-chain nitrogen atom of Leu300 is conserved in the Fidarestat and the 2*R*4*S* structures, an induced rotation in the exocyclic amide group occurred to accommodate the 2*R*4*S* into the binding site, resulting in a short contact with Trp219 (2.79 versus 3.61 Å with Fidarestat). Moreover, a comparison of the IC_{50} values of Fidarestat, the 2*R*4*S*-isomer and Sorbinil for the rat ALR2 (Table 1) suggests that the exocyclic amide group in the *S*-configuration (IC_{50} = 0.035 μM) is optimally positioned to form a hydrogen bond and van der Waals contacts with Leu300 and Trp219, respectively. The missing exocyclic amide group in Sorbinil (IC_{50} = 0.90 μM) and the short contact between the exocyclic amide group of the isomer in the *R* configuration (IC_{50} = 0.57 μM) and the side chain of Trp219 were suggested to account for the weaker binding of both Sorbinil and the 2*R*4*S* isomer to ALR2 [45].

Structure of the Leu300Pro ALR2/Fidarestat complex

To investigate the role of Leu300 of ALR2 in inhibitor selectivity, the mutant form Leu300Pro of ALR2 was prepared and its 3D structure in complex with coenzyme and inhibitor was determined [46]. Fidarestat binds to Leu300Pro ALR2 adopting an orientation similar to that observed previously [44]. The inhibitor's hydantoin moiety is placed deeply into the active site interacting with the residues Tyr48, His110, Trp111 and the cofactor $NADP^+$. The N atom of this

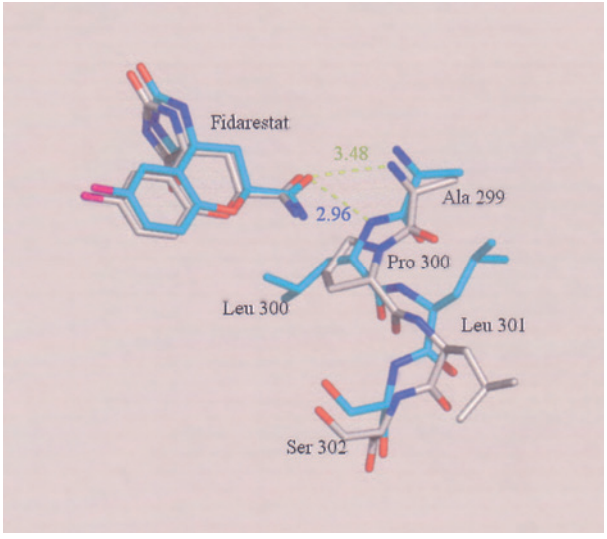

Figure 5. Superposition of the wild-type ALR2 (cyan carbons) and Leu-Pro mutant (grey carbons) residues 299–302 and Fidarestat. Hydrogen bonds are shown as dashed lines, with distances given in Å.

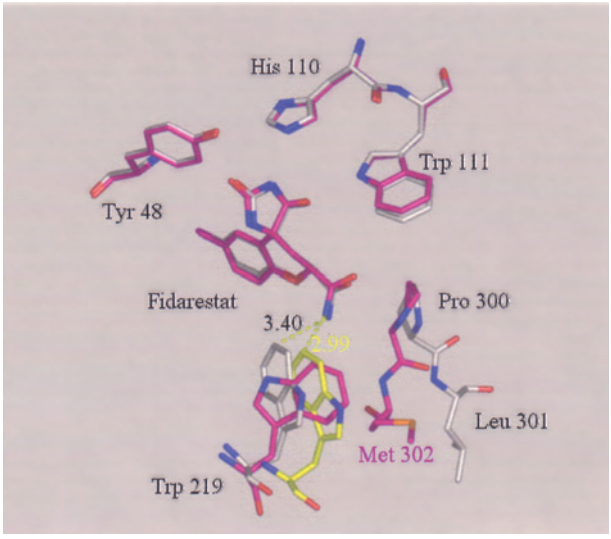

Figure 6. Superposition of the structure of the Leu300Pro ALR2-Fidarestat (grey carbons) complex with the ALR1-Fidarestat complex (magenta carbons, major conformation of Trp220 in yellow carbons) in the active-site region.

moiety is placed at 2.76 Å from the Nε2 atom of His110, while one O atom is at 2.60 Å from the Tyr48 hydroxylate, and the other O atom is at 2.83 Å from the Nε1 atom of Trp111, making H bonds in all cases. At the level of Pro300, the mutation Leu-Pro causes a local shift of residues 299–302 due to the need to accommodate the geometry of the Pro main chain (Fig. 5). The H-bond of the O atom of the Fidarestat amide with the N atom of Leu300 in the wild type (2.96 Å) is lost. There is a contact of 3.48 Å between the O atom of the Fidarestat exocyclic amide and the main-chain N atom of Ala299, but the geometry is not adequate for a proper Hbond. The crystallographic temperature factors (B factors) of the N and O atoms of Fidarestat's exocyclic amide group are larger than those of the remaining part of the inhibitor (~14 $Å^2$ vs ~9 $Å^2$), suggesting that upon loss of the H bond to Leu300, this portion gains higher residual mobility. In comparison, the B factors for these atoms in the Fidarestat-ALR2 complex are of the same order as for the remaining portion of the inhibitor.

The superposition of the structure of the Leu300Pro ALR2-Fidarestat complex with the ALR1-Fidarestat complex in the active-site region (Fig. 6) indicates that the orientation of the inhibitor is very similar in both cases and the interactions of the hydantoin head with active site residues His110, Tyr48 and Trp20 follow the same patterns [43, 46]. The position of Pro300 in ALR2 superimposes with that of Pro301 in ALR1. In both cases, the exocyclic amide moiety of the inhibitor does not form any H bonds with the protein. Instead, close van der Waals contacts occur through different contacting atoms in ALR1 and ALR2 because the flanking side chains of Pro300 (Pro301 in ALR1) and Trp219 (Trp220 in ALR1) reside on the protein backbones that take a slightly different trace in space due to structural and sequential differences [43, 46]. In the case of ALR1, the side chain of Trp220 occupies two conformations of which the minor one (20 % occupancy) has an orientation similar to that observed in the ALR2 structure. The exocyclic amide moiety makes van der Waals contacts with the side chain of Trp220 in both conformations (2.99 Å for the minor and 3.59 Å for the major one). This suggests that the short contact might induce some conformational changes.

The selectivity-determining features in terms of the thermodynamic data were investigated by studying the binding of Fidarestat and Sorbinil, using microcalorimetry, towards wild-type aldose reductase and its Leu300Pro mutant [46]. The binding of the two inhibitors is affected by superimposed changes in protonation states which, in principle, have to be corrected before a subsequent factorization into absolute enthalpic and entropic contributions can be performed. However, assuming that for each individual ligand such protonation effects are identical for wild-type and mutant, a relative comparison of the thermodynamic differences and thus driving forces was attempted for each ligand with respect to the wild-type and Leu300Pro mutant.

The free energy of binding, ΔG°, drops for Fidarestat when comparing the wild type and the Leu300Pro mutant by approximately 8 kJ/mol [46]. When considering the structurally related Sorbinil, virtually identical ΔG° values were observed for the same

pair. Taking the structural difference of the Fidarestat and Sorbinil complexes into account [35, 44], the first inhibitor forms a hydrogen bond via its carbonyl oxygen of the exocyclic amide functional group and the Leu300 backbone NH. In the Leu300Pro-Fidarestat complex, a similar hydrogen bond cannot be formed due to the absence of an NH functionality in proline. Obviously, this loss of a hydrogen bond relates to the ΔG° difference of 8 kJ/mol. Sorbinil lacks an appropriate functional group to hydrogen bond to the main-chain atoms of Leu300; accordingly, the loss of such functionality on the side of the protein due to the Leu300Pro replacement is not experienced by ligand binding. The free energy drop of Fidarestat is mainly attributed to an enthalpy loss, whereas entropy remains nearly unchanged. For Sorbinil, the unchanged ΔG° for both complexes factorizes into mutually compensating enthalpy and entropy changes leading to an enthalpically more favorable and entropically less beneficial binding to the wild type [46].

Inhibitor selectivity between ALR1 and ALR2

The inhibitory activities of Sorbinil against porcine and human ALR1 are similar to those reported for human and rat ALR2 (Table 1), which have a conserved inhibitor-binding site. This is not surprising when considering that Sorbinil lacks the exocyclic amide group which is responsible for the difference in Fidarestat's potency for the two enzymes, and that the hydrogen-bonding interactions between the cyclic imide moiety of the inhibitor and the active-site residues Tyr50, His113 and Trp114 are conserved [43]. Significant selectivity for ALR2 over ALR1 is observed with respect to the more potent ALR2 inhibitors, the 2*R*4*S* isomer and particularly Fidarestat (2*S*4*S*) [43, 45]. The crystal structures of the two enzymes in complex with Fidarestat suggest that the 278-fold difference in the binding of inhibitor to porcine ALR1 and human ALR2 is due to both the additional hydrogen bond present between the main-chain nitrogen atom of Leu300 and the more favoured van der Waals contact between the exocyclic amide group and the side chain of Trp219 in ALR2 [43, 44]. In the case of 2*R*4*S* binding, the inability of Pro301 to form a hydrogen bond with the exocyclic amide group of the compound in porcine ALR1 is the factor that likely accounts for the 31-fold difference in potency with the rat ALR2 [45]. Additionally, similar to ALR2, the *R* configuration of the exocyclic amide group may result in a less favoured interaction with the side chain of Trp220 in ALR1, as suggested by the IC_{50} values [43]. An estimation of the electrostatic interactions between Fidarestat and Tyr50, His113, Trp114 and Leu300 (Pro301 in ALR1) was obtained from molecular modelling (Table 1). The values for the binding enthalpies (ΔH) for porcine ALR1 and human ALR2 were equal to –12 and –15 kcal/mol, with corresponding IC_{50} values of 2.5 and 0.009 μM, respectively [43]. These values, together with the crystal structures, suggest that while the hydrogen-bonding interaction between the main-chain nitrogen atom of Leu300 and the exocyclic amide group of Fidarestat in ALR2 plays an important role in inhibitor binding and selectivity, it does not account for the full difference in the binding for the two enzymes. The only other observed significant difference in the ALR1 and ALR2 structures is the interaction between the exocyclic amide group and the side chain of Trp220, which is ordered in ALR2 but adopts a disordered double conformation in ALR1, with the minor conformation (20 % occupancy) similar to that of Trp219 in ALR2 [43, 44]. Therefore, it is likely that this interaction contributes to a less favoured inhibitor binding to ALR1.

The selectivity advantage of Fidarestat to the Leu300-Pro mutant over the wild type is approximately 23-fold, arising from a ΔG° of 8 kJ/mol [46]. This corresponds essentially to the enthalpy loss of one H bond. However, considering the IC_{50} values for the binding of Fidarestat to ALR2 and ALR1, a larger difference (278-fold) in favour of ALR2 is indicated. This supports the concept that the binding of Fidarestat towards both enzymes is discriminated by additional features, such as the difference attributed to the observed disorder of Trp220 in the ALR1 complex [43]. In the ALR2 mutant case, this residue is well ordered, and makes a favourable contact (3.40 Å) with Fidarestat [44]. In ALR1, this residue adopts at least two conformations, one with a closer contact to Fidarestat (2.99 Å). It is likely that this interaction of Fidarestat with Trp220 in ALR1, together with the loss of one H bond, is responsible for the reduced free energy of binding accounting for the selectivity advantage.

Conclusions

The interaction between ALR1 and the exocyclic amide of Fidarestat results in a disordered split conformation for the side chain of Trp220, making inhibitor binding less favourable compared to ALR2. The H bond of the exocyclic amide group of the inhibitor with Leu300 is lost in the complex structure of the ALR2 Leu300Pro mutant without being compensated by a similar interaction. This hypothesis is supported by the thermodynamic data, as the

predominant difference between mutant and wild type is of enthalpic nature. The H bond towards Leu300 in ALR2 and the split conformation of Trp220 observed in the ALR1 complex are the key determinants for the specificity of Fidarestat for ALR2 over ALR1. Preliminary molecular modelling and design studies suggest that the replacement of the exocyclic amide group of Fidarestat with a carboxylate functional group enhances the net binding energy of the enzyme-inhibitor complex by capturing additional interactions with non-conserved residues from the C-terminal loop of ALR2 [54].

1 Srivastava, S., Spite, M., Trent, J. O., West, M. B., Ahmed, Y. and Bhatnagar, A. (2004) Aldose reductase-catalyzed reduction of aldehyde phospholipids. J. Biol. Chem. 279, 53395 – 53406.

2 Hayashi, H., Fujii, Y., Watanabe, K., Urade, Y. and Hayaishi, O. (1989) Enzymatic conversion of prostaglandin H2 to prostaglandin F2 alpha by aldehyde reductase from human liver: comparison to the prostaglandin F synthetase from bovine lung. J. Biol. Chem. 264, 1036 – 1040.

3 Matsuura, K., Shiraishi, H., Hara, A., Sato, K., Deyashiki, Y., Ninomiya, M. and Sakai, S. (1998) Identification of a principal mRNA species for human 3alpha-hydroxysteroid dehydrogenase isoform (AKR1C3) that exhibits high prostaglandin D2 11-ketoreductase activity. J. Biochem. (Tokyo) 124, 940 – 946.

4 Hung, C. F. and Penning, T. M. (1999) Members of the nuclear factor 1 transcription factor family regulate rat 3alpha-hydroxysteroid/dihydrodiol dehydrogenase (3alpha-HSD/DD AKR1C9) gene expression: a member of the aldo-keto reductase superfamily. Mol. Endocrinol. 13, 1704 – 1717.

5 Nelson, V. L., Qin Kn, K. N., Rosenfield, R. L., Wood, J. R., Penning, T. M., Legro, R. S., Strauss, J. F. 3rd and McAllister, J. M. (2001) The biochemical basis for increased testosterone production in theca cells propagated from patients with polycystic ovary syndrome. J. Clin. Endocrinol. Metab. 86, 5925 – 5933.

6 Gavidia, I., Perez-Bermudez, P. and Seitz, H. U. (2002) Cloning and expression of two novel aldo-keto reductases from *Digitalis purpurea* leaves. Eur. J. Biochem. 269, 2842 – 2850.

7 Steckelbroeck, S., Jin, Y., Oyesanmi, B., Kloosterboer, H. J. and Penning, T. M. (2004) Tibolone is metabolized by the 3alpha/3beta-hydroxysteroid dehydrogenase activities of the four human isozymes of the aldo-keto reductase 1C subfamily: inversion of stereospecificity with a delta5(10)-3-ketosteroid. Mol. Pharmacol. 66, 1702 – 1711.

8 Ji, Q., Aoyama, C., Nien, Y. D., Liu, P. I., Chen, P. K., Chang, L., Stanczyk, F. Z. and Stolz, A. (2004) Selective loss of AKR1C1 and AKR1C2 in breast cancer and their potential effect on progesterone signaling. Cancer Res. 64, 7610 – 7617.

9 Hara, A., Deyashiki, Y., Nakayama, T. and Sawada, H. (1983) Isolation and characterization of multiforms of aldehyde reductase in chicken kidney. Eur. J. Biochem. 133, 207 – 214.

10 Sawada, H., Hara, A., Nakayama, T. and Kato, F. (1980) Reductases for aromatic aldehydes and ketones from rabbit liver: purification and characterization. J. Biochem. (Tokyo) 87, 1153 – 1165.

11 Wermuth, B., Munch, J. D. and von Wartburg, J. P. (1977) Purification and properties of NADPH-dependent aldehyde reductase from human liver. J. Biol. Chem. 252, 3821 – 3828.

12 Sawada, H., Hara, A., Nakayama, T. and Hayashibara, M. (1982) Kinetic mechanisms in the reduction of aldehydes and ketones catalyzed by rabbit liver aldehyde reductases and hydroxysteroid dehydrogenases. J. Biochem. (Tokyo) 92, 185 – 191.

13 Jez, J. M., Flynn, T. G. and Penning, T. M. (1997) A new nomenclature for the aldo-keto reductase superfamily. Biochem. Pharmacol. 54, 639 – 647.

14 Warren, J. C., Murdock, G. L., Ma, Y., Goodman, S. R. and Zimmer, W. E. (1993) Molecular cloning of testicular 20 alpha-hydroxysteroid dehydrogenase: identity with aldose reductase. Biochemistry 32, 1401 – 1406.

15 Dixit, B. L., Balendiran, G. K., Watowich, S. J., Srivastava, S., Ramana, K. V., Petrash, J. M., Bhatnagar, A. and Srivastava, S. K. (2000) Kinetic and structural characterization of the glutathione-binding site of aldose reductase. J. Biol. Chem. 275, 21587 – 21595.

16 Tabakoff, B. and Erwin, V. G. (1970) Purification and characterization of a reduced nicotinamide adenine dinucleotide phosphate-linked aldehyde reductase from brain. J. Biol. Chem. 245, 3263 – 3268.

17 Tulsiani, D. R. and Touster, O. (1977) Resolution and partial characterization of two aldehyde reductases of mammalian liver. J. Biol. Chem. 252, 2545 – 2550.

18 Flynn, T. G., Shires, J. and Walton, D. J. (1975) Properties of the nicotinamide adenine dinucleotide phosphate-dependent aldehyde reductase from pig kidney: amino acid composition, reactivity of cysteinyl residues, and stereochemistry of D-glyceraldehyde reduction. J. Biol. Chem. 250, 2933 – 2940.

19 Dunlop, M. (2000) Aldose reductase and the role of the polyol pathway in diabetic nephropathy. Kidney Int. Suppl. 77, S3 – S12.

20 Kinoshita, J. H. and Nishimura, C. (1988) The involvement of aldose reductase in diabetic complications. Diabetes Metab. Rev. 4, 323 – 337.

21 Yabe-Nishimura, C. (1998) Aldose reductase in glucose toxicity: a potential target for the prevention of diabetic complications. Pharmacol. Rev. 50, 21 – 33.

22 Costantino, L., Rastelli, G., Gamberini, M. C. and Barlocco, D. (2000) Pharmacological approaches to the treatment of diabetic complications. Exp. Opin. Ther. Pat. 10, 1245 – 1262.

23 Oates, P. J. and Mylari, B. L. (1999) Aldose reductase inhibitors: therapeutic implications for diabetic complications. Exp. Opin. Invest. Drugs 8, 1 – 25.

24 Pfeifer, M. A., Schumer, M. P. and Gelber, D. A. (1997) Aldose reductase inhibitors: the end of an era or the need for different trial design. Diabetes 46, S82 – S89.

25 Miyamoto, S. (2002) Recent advances in aldose reductase inhibitors: potential agents for the treatment of diabetic complications. Exp. Opin. Ther. Pat. 12, 621 – 631.

26 El-Kabbani, O., Wilson, D. K., Petrash, M. and Quiocho, F. A. (1998) Structural features of the aldose reductase and aldehyde reductase inhibitor-binding sites. Mol. Vis. 4, 19 – 25.

27 Bohren, K. M., Grimshaw, C. E. and Gabbay, K. H. (1992) Catalytic effectiveness of human aldose reductase: critical role of C-terminal domain. J. Biol. Chem. 267, 20965 – 20970.

28 Barski, O. A., Gabbay, K. H. and Bohren, K. M. (1996) The C-terminal loop of aldehyde reductase determines the substrate and inhibitor specificity. Biochemistry 35, 14276 – 14280.

29 Sato, S. and Kador, P. F. (1990) Inhibition of aldehyde reductase by aldose reductase inhibitors. Biochem. Pharmacol. 40, 1033 – 1042.

30 Feather, M. S., Flynn, T. G., Munro, K. A., Kubiseski, T. J. and Walton, D. J. (1995) Catalysis of reduction of carbohydrate 2-oxoaldehydes (osones) by mammalian aldose reductase and aldehyde reductase. Biochim. Biophys. Acta 1244, 10 – 16.

31 Ratliff, D. M., Van der Jagt, D. J., Eaton, R. P. and Van der Jagt, D. L. (1996) Increased levels of methylglyoxal-metabolizing enzymes in mononuclear and polymorphonuclear cells from insulin-dependent diabetic patients with diabetic complications: aldose reductase, glyoxalase I, and glyoxalase II – a clinical research center study. J. Clin. Endocrinol. Metab. 81, 488 – 492.

32 Da Settimo, F., Primofiore, G., Da Settimo, A., La Motta, C., Taliani, S., Simorini, F., Novellino, E., Greco, G., Lavecchia, A. and Boldrini, E. (2001) [1,2,4]Triazino[4,3-a]benzimidazole

acetic acid derivatives: a new class of selective aldose reductase inhibitors. J. Med. Chem. 44, 4359 – 4369.
33 Oka, M., Matsumoto, Y., Sugiyama, S., Tsuruta, N. and Matsushima, M. (2000) A potent aldose reductase inhibitor, (2S,4S)-6-fluoro-2′,5′-dioxyspiro[chroman-4,4′-imidazoline]-2-carboxamide (Fidarestat): its absolute configuration and interaction with aldose reductase by X-ray crystallography. J. Med. Chem. 43, 2479 – 2483.
34 Kurono, M., Fujiwara, I. and Yoshida, K. (2001) Stereospecific interaction of a novel spirosuccinimide type aldose reductase inhibitor, AS-3201, with aldose reductase. Biochemistry 40, 8216 – 8226.
35 Urzhumtsev, A., Tête-Favier, F., Mitschler, A., Barbanton, J., Barth, P., Urzhumtseva, L., Biellmann, J. F., Podjarny, A. and Moras, D. (1997) 'Specificity' pocket inferred from the crystal structures of the complexes of aldose reductase with the pharmaceutically important inhibitors tolrestat and sorbinil. Structure 5, 601 – 612.
36 Sarges, R. and Oates, P. J. (1993) Aldose reductase inhibitors: recent developments. Prog. Drug Res. 40, 99 – 161.
37 Eggler, J. F., Larson, E. R., Lipinski, C. A., Mylari, B. L. and Urban, F. J. (1993) A perspective of aldose reductase inhibitors. In: Advances in Medicinal Chemistry, vol. 2, pp. 197 – 246. Jai, Greenwich.
38 Larson, E. R., Lipinski, C. A. and Sarges, R. (1988) Medicinal chemistry of aldose reductase inhibitors. Med. Chem. Rev. 8, 159 – 186.
39 El-Kabbani, O., Carper, D. A., McGowan, M. H., Devedjiev, Y., Rees-Milton, K. J. and Flynn, T. G. (1997) Studies on the inhibitor-binding site of porcine aldehyde reductase: crystal structure of the holoenzyme-inhibitor ternary complex. Proteins Struct. Funct. Genet. 29, 186 – 192.
40 El-Kabbani, O., Old, S. E., Ginell, S. L. and Carper, D. A. (1999) Aldose and aldehyde reductases: structure-function studies on the coenzyme and inhibitor-binding sites. Mol. Vis. 5, 20 – 26.
41 Jez, J. M., Bennett, M. J., Schlegel, B. P., Lewis, M. and Penning, T. M. (1997) Comparative anatomy of the aldo-keto reductase superfamily. Biochem. J. 326, 625 – 636.
42 El-Kabbani, O., Rogniaux, H., Barth, P., Chung, R. P.-T., Fletcher, E., Dorsselaer, A. and Podjarny, A. (2000) Aldose and aldehyde reductases: correlation of molecular modelling and mass spectrometric studies on the binding of inhibitors to the active site. Proteins Struct. Funct. Genet. 41, 407 – 414.
43 El-Kabbani, O., Carbone, V., Darmanin, C., Oka, M., Mitschler, A., Podjarny, A., Schulze-Briese, C. and Chung, R. P.-T. (2005) Structure of aldehyde reductase holoenzyme in complex with the potent aldose reductase inhibitor Fidarestat: implications for inhibitor binding and selectivity. J. Med. Chem. 48, 5536 – 5542.
44 El-Kabbani, O., Darmanin, C., Schneider, T. R., Hazemann, I., Ruiz, F., Oka, M., Joachimiak, A., Schulze-Briese, C., Tomizaki, T., Mitschler, A. and Podjarny, A. (2004) Ultra high-resolution structures of human aldose reductase holoenzyme complexed with Fidarestat and Minalrestat: implications for the binding of cyclic imide inhibitors. Proteins 55, 805 – 813.
45 El-Kabbani, O., Darmanin, C., Oka, M., Schulze-Briese, C., Tomizaki, T., Hazemann, I., Mitschler, A. and Podjarny, A. (2004) High resolution structures of human aldose reductase holoenzyme in complex with stereoisomers of the potent inhibitor Fidarestat: stereospecific interaction between the enzyme and a cyclic imide inhibitor. J. Med. Chem. 47, 4530 – 4537.
46 Petrova, T., Steuber, H., Hazemann, I., Cousido-Siah, A., Mitschler, A., Chung, R., Oka, M., Klebe, G., El-Kabbani, O., Joachimiak, A. and Podjarny, A. (2005) Factorizing selectivity determinants of inhibitor binding towards aldose and aldehyde reductases: structural and thermodynamic properties of the aldose reductase mutant Leu300Pro/Fidarestat complex. J. Med. Chem. 48, 5659 – 5665.
47 Rondeau, J.-M., Tête-Favier, F., Podjarny, A., Reymann, J.-M., Barth, P., Biellmann, J.-F. and Moras, D. (1992) Novel NADPH-binding domain revealed by the crystal structure of aldose reductase. Nature 355, 469 – 472.
48 Malamas, M. S., Hohman, T. C. and Millen, J. (1994) Novel spirosuccinimide aldose reductase inhibitors derived from isoquinoline-1,3-diones:2[(4-bromo-2-fluorophenyl)methyl]-6-fluoro-spiro [isoquinoline-4(1H),3'-pyrrolidine]-1,2',3,5'(2H)-tetrone and congeners. J. Med. Chem. 37, 2043 – 2058.
49 Malamas, M. S. and Hohman, T. C. (1994) N-substituted spirosuccinimide, spiropyridazine, spiroazetidine and acetic acid aldose reductase inhibitors derived from isoquinoline-1, 3-diones. J. Med. Chem. 37, 2059 – 2070.
50 Negoro, T., Murata, M., Ueda, S., Fujitani, B., Ono, Y., Kuromiya, A., Komiya, M., Suzuki, K. and Matsumoto, J. (1998) Novel, highly potent aldose reductase inhibitors: R-(–)-2-(4-bromo-2-fluorobenzyl)-1,2,3,4-tetrahydropyrrolo[1,2-a]pyrazine-4-spiro-3'-pyrolidine-1,2',3,5-tetrone (AS-3201) and its congeners. J. Med. Chem. 41, 4118 – 4129.
51 Grimshaw, C. E., Bohren, K. M., Lai, C.J. and Gabbay, K. H. (1995) Human aldose reductase: pK of tyrosine 48 reveals the preferred ionization state for catalysis and inhibition. Biochemistry 34, 14374 – 14384.
52 Ehrig, T., Bohren, K. M., Prendergast, F. G. and Gabbay, K. H. (1994) Mechanism of aldose reductase inhibition: binding of $NADP^+$/NADPH and alrestatin like inhibitors. Biochemistry 33, 7157 – 7165.
53 Ashizawa, N. and Aotsuka, T. (1998) Benzothiazole aldose reductase inhibitors. Drugs Fut. 23, 521 – 529.
54 Darmanin, C., Chevreux, G., Potier, N., Van Dorsselaer, A., Hazemann, I., Podjarny, A. and El-Kabbani, O. (2004) Probing the ultra-high resolution structure of aldose reductase with molecular modelling and noncovalent mass spectrometry. Bioorg. Med. Chem. 12, 3797 – 3806.
55 Mizuno, K., Yamaguchi, T., Unoue, A., Tomiya, N., Unno, R., Miura, K., Usui, T., Matsumoto, Y., Kondo, Y., Yoshina, S., Kondo, Y., Sato, M., Matsubara, A., Kato, N., Nakano, K., Shirai, M., Inoue, T., Awaya, J., Asaeda, N., Hayasaka, I., Koide, M., Hibi, C., Ban, M., Sawai, K. and Kurono, M. (1990) Profile of a new aldose reductase inhibitor (2S,4S)-6-fluoro-2′,5′-dioxyspiro[chroman-4,4′-imidazoline]-2-carboxamide. Excerpta Med. 913, 89 – 96.
56 Barski, O. A., Gabbay, K. H., Grimshaw, C. E. and Bohren, K. M. (1995) Mechanism of human aldose reductase: characterization of the active site pocket. Biochemistry 34, 11264 – 11275.
57 Yamaguchi, T., Miura, K., Usui, T., Unno, R., Matsumoto, Y., Fukushima, M., Mizuno, K., Kondo, Y., Baba, Y. and Kurono, M. (1994) Synthesis and aldose reductase inhibitory activity of 2-substituted-6-fluoro-2,3-dihydrospiro [4H-1-benzopyran-4, 4'-imidazolidine]-2',5'-diones. Arzneim. Forsch. Drug Res. 44, 344 – 348.